Check for updates

In situ strategy to prepare PDPB/SnO$_2$ p–n heterojunction with a high photocatalytic activity

Yuhang Wang, Yuanxin Deng, Linggang Fan, Yu Zhao, Bin Shen, Di Wu, Yi Zhou, Chencheng Dong, Mingyang Xing* and Jinlong Zhang [ID] *

As a novel material for water depollution, conjugated polydiphenylbutadiyne (PDPB) nanofibers have received attention due to their visible light responsive photocatalytic activity. In this study, we successfully prepared a PDPB/SnO$_2$ p–n heterojunction by an *in situ* growth route. The XPS characterization indicates the generation of Sn–C bonds between SnO$_2$ and PDPB, which would decrease the bandgap of SnO$_2$ and promote the transference efficiency of electrons and holes between these two components. The PDPB could act as the sensitizer to enlarge the solar light absorption region of the heterojunction. The SnO$_2$ provides a stable mesoporous structure and enhanced hydrophilic properties. The solar-driven photodegradation rate of Rhodamine B over the PDPB/SnO$_2$ (ratio is 2 : 1) is 4 times higher than that of the pure SnO$_2$ and 2 times higher than that of the pure PDPB nanofibers. Our strategy gives a facile strategy for the preparation of an organic–inorganic hybrid heterojunction with high solar light activity.

1. Introduction

In recent years, SnO$_2$ mesoporous single crystals (MSCs) have gained much attention due to their excellent properties such as perfect single-crystallinity, large specific surface areas, high electron mobility and exposed active sites.[1–4] These advantages have led to the successful research for their various applications in photocatalysis,[5,6] sensors[7–9] and solar cells.[10,11] However, SnO$_2$ MSCs have an inevitable drawback ascribed to their wide band gap, which limits solar light from being absorbed and then leads to the low photocatalytic activity. Thus, it is urgent to find a strategy to extend the light harvesting of SnO$_2$ MSCs. Much effort has been focused on enhancing the photoabsorption and the charge separation rate of SnO$_2$ by methods such as element doping,[12,13] surface modification,[14,15] and heterojunction design.[16–18] Note that coupling of two materials as a semiconductor heterojunction could substantially improve the photocatalytic activity by broadening the absorption range of light and increasing the separation efficiency of the photogenerated electrons and holes.[19–23] Zhang et al.[24] used a one-step fabrication to synthesize an Ag$_3$PO$_4$/SnO$_2$ composite, which showed improved photocatalytic activity and structural stability for photodecomposition of organic compounds. Zheng et al.[25] synthesized a network structured SnO$_2$/ZnO nanocatalyst by a two-step solvothermal method. The photocatalytic activity of

SnO$_2$/ZnO for the degradation of methyl orange was much higher than that of the pure SnO$_2$ and ZnO. Zhang et al.[26] used a combination method of sol–gel process and electrospinning technique to synthesize the one-dimensional ZnO–SnO$_2$ nanofibers, which exhibited excellent photocatalytic activity, superior to the electrospun pure ZnO and SnO$_2$ nanoparticles. According to these published studies, the heterojunction structure of two semiconductors will open an efficient pathway for the improvement of photocatalytic activity and stability.

Recently, conjugated polymer polydiphenylbutadiyne (PDPB) nanofibers[27] attracted wide attention due to their high visible light response, stable cycling property and low cost. They have a narrow band gap of 1.81 eV, which is attributed to the octamer structure. The electrons could be generated by the conjugated polymer chains when illuminated by energetic photons, but PDPB nanofibers have a highly hydrophobic feature that limits their photocatalytic performance in water. In order to overcome these drawbacks, we synthesized a p–n heterojunction structure of SnO$_2$ and PDPB. In this heterojunction structure system, PDPB nanofibers could enlarge the spectral absorption range, whereas SnO$_2$ MSCs could provide a stable mesoporous structure and a hydrophilic environment.

Herein, we employed a facile and green *in situ* strategy to synthesize a PDPB/SnO$_2$ heterojunction. This heterojunction has advantages of both single crystals and polymers, such as high photosensitivity, stable mesoporous structure and good hydrophilicity. The PDPB nanofibers were adsorbed and grown on the surface of the SnO$_2$ MSCs, and the Sn–C bonds were generated between them to realize the carbon doping on SnO$_2$. When the heterojunction surface was illuminated, PDPB

Key Laboratory for Advanced Materials, Institute of Fine Chemicals, School of Chemistry & Molecular Engineering, East China University of Science and Technology, 130 Meilong Road, Shanghai 200237, P. R. China. E-mail: mingyangxing@ecust.edu.cn; jlzhang@ecust.edu.cn

nanofibers absorbed the light and generated electrons. Moreover, carbon-doped SnO_2 (C–SnO_2) MSCs offered charge transfer channels, which endowed the PDPB/SnO_2 composites with a high photocatalytic activity. The photodegradation rate of Rhodamine B (RhB) over the PDPB/SnO_2 composite (ratio is 2 : 1) is 4 times that of the single SnO_2 MSCs and 2 times that of single PDPB nanofibers.

2. Experimental

2.1 Materials

Tetraethyl orthosilicate (TEOS), aqueous solution of ammonia ($NH_3 \cdot H_2O$, 25 wt%), ethanol, distilled water, stannic chloride ($SnCl_4 \cdot 5H_2O$), polyethylene pyrrole (PVP), hydrochloric acid (HCl), sodium hydroxide (NaOH), sodium chloride, sodium dodecyl sulphate, 1,4-diphenylbutadiyne (DPB), benzoin methyl ether (BME), cyclohexane, and pentanol-1 were used. All chemicals were of analytical grade and used without further purification.

2.2 Preparation of photocatalysts

Preparation of SiO_2 spheres. The silica spheres were synthesized by the Stöber method. First, 167.2 mL ethanol was mixed with 28.8 mL water in a beaker. The mixture was stirred for 1 min at room temperature. Simultaneously, 18.0 mL tetraethoxysilane (TEOS) was mixed with 182.0 mL absolute ethanol at room temperature. The TEOS solution was stirred for 1 min and poured into the abovementioned mixture. After that, 4.0 mL ammonium hydroxide solution was added into the mixture. The precursor liquid was stirred for 24 h to obtain a suspension (silica colloids). Then, it was centrifuged at 12 000 rpm for 1 h and dried in a vacuum oven at 60 °C for 12 h.

Preparation of SnO_2 MSCs. The SnO_2 MSCs were prepared by a modifying the method developed by Zheng *et al.*[28] Herein, 12 mL H_2O, 12 mL ethanol and 0.1 g PVP were added in the autoclave (50 mL volume). After being completely dissolved, 1.346 g $SnCl_4 \cdot 5H_2O$ was added into the autoclave. Then, the mixture was stirred at room temperature for 10 min, and 1.8 mL hydrochloric acid (HCl, 37%) was added and stirred for another 10 min. Then, 0.8 g SiO_2 was added, and the sealed vessel was heated at 200 °C for 12 h. Finally, the silica template was removed by etching in 2 M NaOH at 80 °C for 1 h. The remaining products were collected by centrifugation and washed several times with H_2O and ethanol.

Preparation of PDPB/SnO_2 MSC heterojunction. The *in situ* route to PDPB/SnO_2 MSCs was prepared by modifying the method developed by Ghosh *et al.*[27] Herein, 0.035 g NaCl was dissolved in 2 mL H_2O, and 1 g of a surfactant (sodium dodecyl sulphate) was dissolved in the mixture solution. After vigorous agitation for 5 h, the surfactant had completely dissolved to form a transparent and viscous micellar solution. After that, we weighed 0.1 g DPB and 0.01 g BME into a beaker and added 5 mL cyclohexane, followed by ultrasound treatment of the solution for complete dissolution. This solution was added to the abovementioned micellar solution under stirring, which led to a white unstable emulsion. After reaction for 0.5 h, a co-

surfactant, pentanol-1 (420 μL) was added to the mixture and stirred for 3 h. Then, different masses of SnO_2 MSCs were added into the mixture. The glass tube was illuminated using a 300 W xenon lamp at a distance of 5 cm for 12 h. Then, the products were extracted into a 15 mL water and 15 mL ethanol solution and dried in a vacuum oven at 60 °C for 12 h.

2.3 Characterizations

The crystal structure of the sample was detected by X-ray diffraction (XRD) measurements (Rigaku Ultima IV (Cu Kα radiation, $\lambda = 1.5406$ Å) in the range of 10–80° (2θ)). The morphologies of the PDPB/SnO_2 heterojunctions were characterized by transmission electron microscopy (TEM, JEM2100) and field emission scanning electron microscopy (FESEM, HITACHI, S4800). BET specific surface area measurements were studied by N_2 adsorption at 77 K using an ASAP2020 instrument. The X-ray photoelectron spectroscopy (XPS) studies were carried out using a Perkin-Elmer PHI 5000C ESCA system with Al Kα radiation. The binding energy shift was referenced to the C1s level at 284.6 eV as an internal standard. Infrared spectra (IR) were recorded with KBr disks containing the powder sample with an FTIR spectrometer (Nicolet Magna 550). Thermogravimetric and differential thermal analyses were conducted on a Pyris Diamond TG/DTA (PerkinElmer) apparatus at a heating rate of 20 K min⁻¹ from 40 °C to 800 °C in air flow. UV-vis diffuse reflectance spectra (DRS) were obtained with a SHIMADZU UV-2600 spectroscope equipped with an integrating sphere assembly and using $BaSO_4$ as the reflectance sample. Photocurrent measurements were carried out on an electrochemical analyzer (CHI 660 D electrochemical station, CHI Instruments Inc.) at room temperature. Transient photocurrent responses of different samples were carried out in 0.5 M Na_2SO_4 aqueous solution under various irradiation conditions (300 W Xe lamp).

2.4 Measurements of photocatalytic activity

The photocatalytic activities of the PDPB/SnO_2 MSCs have been evaluated for the photodecomposition of RhB in water. The photocatalyst (0.01 g) was added into a 100 mL quartz photoreactor containing 50 mL of RhB solution (10 mg L⁻¹). The suspension containing PDPB/SnO_2 with pollutants was stirred in the dark for 1 h to establish adsorption–desorption equilibrium before irradiation. A 300 W Xe lamp with an AM1.5 air mass filter was used as a simulated solar light source. Then, the solutions were irradiated for 3 h and quantified every 30 min. The degradation efficiency of RhB was detected by ultraviolet-visible spectrophotometry.

3. Results and discussion

The overall synthesis of the PDPB/SnO_2 MSCs heterojunction consisted of two steps (Scheme 1). First, we used a hard template method to synthesize the SnO_2 MSCs by a solvothermal process. SnO_2 was generated in the gap of the silica template, and the silica was etched by NaOH to form the mesoporous structure of SnO_2. Second, the SnO_2 MSCs were added into the soft template hexagonal mesophases, which contained
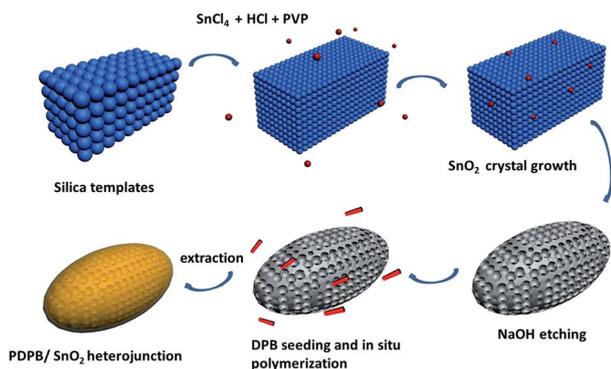
Scheme 1 Synthetic steps of SnO_2 MSCs and PDPB/SnO_2 MSC heterojunction.

DPB and BME. After that, the DPB would grow and adsorb on the surface of SnO_2 MSCs under light irradiation. We synthesized the PDPB/SnO_2 heterojunction with different weight ratios (PDPB : SnO_2 = 4 : 1, 2 : 1, 1.33 : 1, 1 : 1).

3.1 Heterojunction structure

The crystal structures of the PDPB/SnO_2 MSCs were examined by X-ray diffraction (XRD). Fig. 1 shows the XRD patterns of pure SnO_2 MSCs, pure PDPB nanofibers and PDPB/SnO_2 composites. The SnO_2 MSCs showed a rutile phase of tetragonal SnO_2. The sharp peaks are observed at $2\theta = 26.58°, 33.9°, 37.92°, 51.76°, 54.7°, 57.9°, 61.86°, 64.78°$ and $65.92°$, which could be indexed as the (110), (101), (200), (211), (220), (002), (310), (312) and (301) diffraction planes, respectively. The characteristic peaks of PDPB nanofibers also appeared in XRD patterns. There is no evident peak ascribed to the PDPB over the PDPB/SnO_2 composite, which is due to the low loading content of PDPB on the surface of SnO_2.

3.2 Morphology and surface area

The morphologies of the SnO_2 MSCs and PDPB/SnO_2 composites were analyzed by TEM and FESEM, and the results are shown in Fig. 2. From Fig. 2a and c, we can find the obvious, well-defined, and uniform mesoporous structure of the shuttle shape SnO_2 from the TEM and FESEM images. The length and
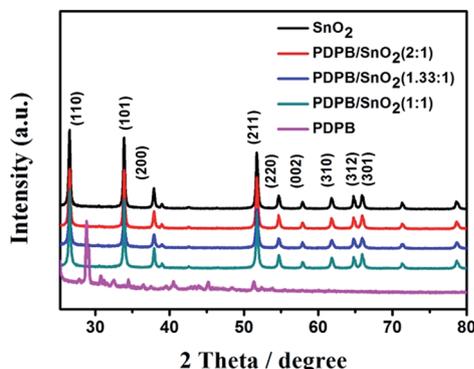

Fig. 1 XRD patterns of pure PDPB, pure SnO_2 and PDPB/SnO_2 composites.
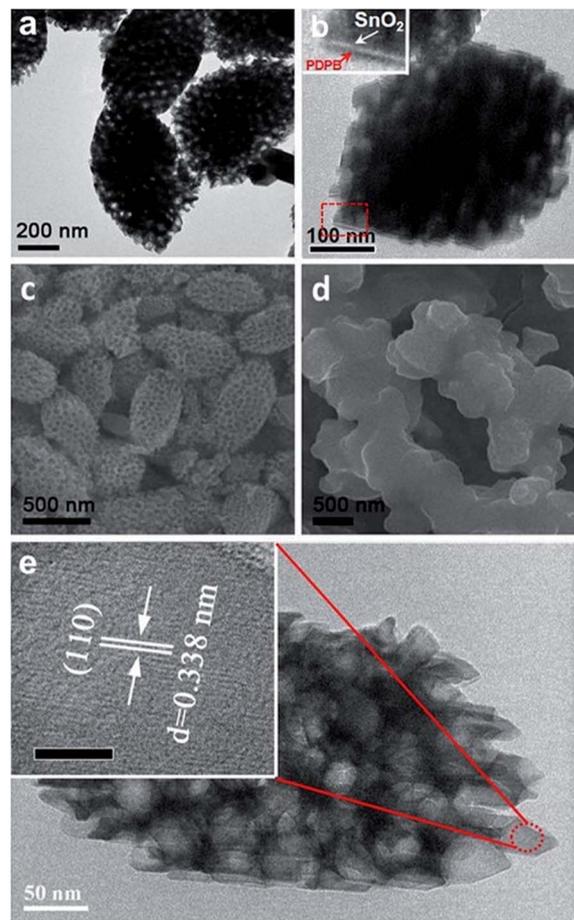

Fig. 2 Morphology characterization results of as-prepared samples. TEM images of pure SnO_2 MSCs (a) and PDPB/SnO_2 composites (2 : 1) (inset is the amplification of the red circle) (b); FESEM images of pure SnO_2 MSCs (c) and PDPB/SnO_2 composites (2 : 1) (d); HRTEM image of SnO_2 MSCs (e).

width of the SnO_2 MSCs are ∼400 nm and ∼200 nm, respectively, and the pore size is uniform at ∼50 nm. The HRTEM images of SnO_2 MSCs (Fig. 2e) show that the uniform lattice distance is 0.338 nm, which indicates the (110) plane of SnO_2. Compared to pure SnO_2 MSCs, Fig. 2b and d demonstrate that the pore structure of PDPB/SnO_2 becomes hazy, which is attributed to the *in situ* growth of PDPB on the surface of SnO_2 MCMs. This speculation is confirmed by the BET results. The BET curve is shown in Fig. 3; the hysteresis loop and the pore size distribution curve could prove that the PDPB does not enter into the pore structure of SnO_2 MSCs. The BET surface area of pure SnO_2 MSCs and PDPB/SnO_2 is 23.2 $m^2\,g^{-1}$ and 31.2 $m^2\,g^{-1}$, respectively, indicating that the PDPB was covered on the surface rather than in the pores of SnO_2. The surface area of PDPB/SnO_2 is a little larger compared to the pure SnO_2, which also implies that the loading of PDPB could not change the original mesoporous structure of SnO_2.

3.3 XPS characterization

The surface composition and chemical states of SnO_2 MSCs and PDPB/SnO_2 composites were investigated by XPS spectra. Fig. 4
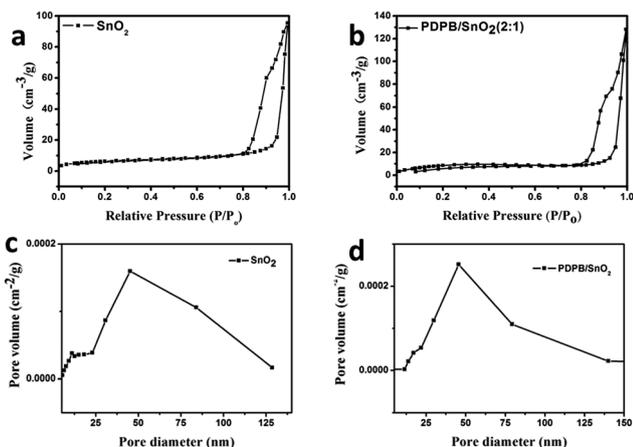
Fig. 3 Nitrogen adsorption/desorption isotherm of SnO_2 MSCs (a) and PDPB/SnO_2 composites (b); pore size distributions of SnO_2 MSCs (c) and PDPB/SnO_2 composites (d).
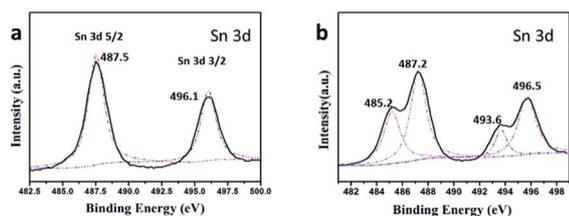

Fig. 4 Sn 3d XPS spectra of pure SnO_2 (a) and PDPB/SnO_2 composites (2 : 1) (b).

shows the Sn 3d XPS spectrum of SnO_2 MSCs and PDPB/SnO_2 composites. The peaks at 487.5 eV and 496.1 eV belong to the Sn $3d_{5/2}$ and Sn $3d_{3/2}$, respectively, which are the characteristic peaks of Sn(IV). Interestingly, compared to pure SnO_2, the Sn 3d spectrum of PDPB/SnO_2 has two extra peaks at 485.2 eV and 493.6 eV. These two peaks indicate the changes of chemical states of Sn element, which may be caused by the combination between SnO_2 and PDPB. A similar phenomenon was also reported in previous literature.[29] We inferred that this result is due to the combination between SnO_2 and PDPB and it may generate a new impurity level with the Sn–C bond. C replaced O from SnO_2 and acted as the electron donor to enlarge the electron cloud density of Sn element, which led to the appearance of new XPS peaks at a lower binding energy.

3.4 IR and TGA analysis

In order to confirm the existence of PDPB and find the interaction between SnO_2 and PDPB, IR spectra were obtained, as shown in Fig. 5. The pure PDPB shows the characteristic peaks at 2850 cm^{-1}, 2919 cm^{-1} and 3048 cm^{-1}, which can be attributed to the C–H vibration of the polymer molecule chains. There are no significant peaks of pure SnO_2 in this region. Compared to the pure SnO_2 and PDPB, the characteristic peaks at 2850 cm^{-1} and 2919 cm^{-1} are consistent with the pure PDPB, but the 3048 cm^{-1} peak is too weak to locate and could be induced by the chemical bonding between SnO_2 and PDPB. The XPS results
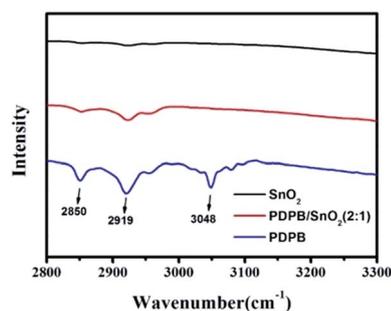

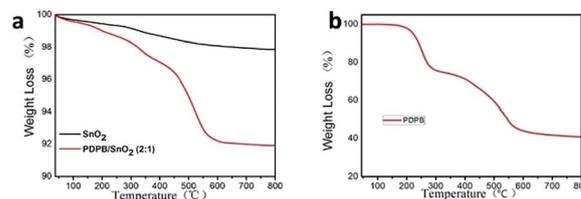Fig. 5 IR spectra of pure SnO_2, pure PDPB and PDPB/SnO_2 composites (2 : 1).

Fig. 6 (a) TGA spectra of SnO_2 and PDPB/SnO_2 composites (2 : 1). (b) TGA spectra of PDPB nanofibers.

indicate the generation of Sn–C bonds between polymers and semiconductors, which could be formed by the dehydration between C–H bonds and Sn–OH bonds.

The loading content of PDPB in the heterojunction was examined by the thermogravimetric analysis (TGA). Fig. 6a demonstrates that the TGA curve of pure SnO_2 is like a horizontal line, indicating the stable property of SnO_2. The curve of the PDPB/SnO_2 heterojunction shows a weight loss at 160 °C. The loss process has two steps: (1) from 160 °C to 250 °C, it indicates the thermal decomposition of polymer chains; (2) from 250 °C to 450 °C, it indicates the decomposition of carbons. From the TGA results, it is observed that PDPB mass in the heterojunction is about 8% (2 : 1 ratio), and the interaction between PDPB and SnO_2 causes the heterojunction (160 °C) to have a weight-loss temperature lower than that of the pure PDPB (200 °C) (Fig. 6b).
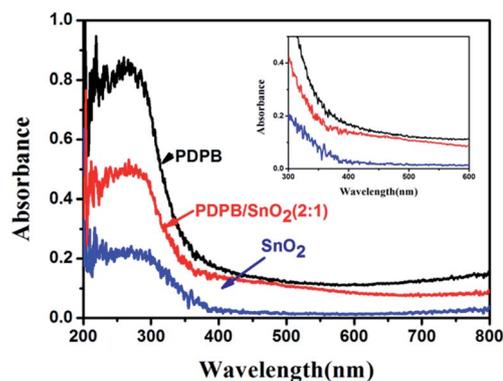

Fig. 7 UV-vis diffuse reflectance spectra of pure PDPB, pure SnO_2 MSCs and PDPB/SnO_2 composites (2 : 1).

3.5 UV-vis diffuse reflectance spectra

The absorbance of the pure SnO_2 MSCs, pure PDPB and PDPB/SnO_2 composites were measured by UV-vis diffuse reflectance spectra (Fig. 7). The pure PDPB shows a high absorption from 200–700 nm wavelength, which shows the excellent light harvest. The PDPB/SnO_2 composites present a lower photo response than pure PDPB due to the low loading amounts of PDPB in the composites. It is clear that the PDPB/SnO_2 composite has a higher absorption value than the pure SnO_2 MSCs from 200–700 nm wavelengths. Particularly in the ultraviolet region, the absorption value over heterojunction has a remarkable increase than the pure SnO_2 MSCs, which indicates that PDPB could enhance the light absorption of SnO_2. From the UV-vis results, we can demonstrate that PDPB could be used as the sensitizer to enlarge the solar light response range of SnO_2, which is expected to improve the photocatalytic activity of SnO_2 under solar light.

3.6 Photochemical property measurement

In order to compare the photochemical properties of pure SnO_2 and PDPB/SnO_2 composites, we used the transient photocurrent response measurements to characterize the separation efficiency of photogenerated electrons and holes. The photocurrents of these samples were recorded in the dark or under solar light illumination using the xenon lamp assembled with an AM1.5 optical filter as the light source, as shown in Fig. 8. The results show that the photocurrent of PDPB/SnO_2 is much higher than that of pure SnO_2 MSCs. For PDPB/SnO_2 composites, the photocurrent response was 4 μA cm^{-2}, which is about 4 times that of the SnO_2 MSCs (below 1 μA cm^{-2}). As we know, carbon-doped SnO_2 is the n-type semiconductor and PDPB is the p-type polymer semiconductor.[30] Owing to the p–n heterojunction structure of PDPB and SnO_2 MSCs, the composites display a higher transfer rate of photogenerated electron–hole pairs, which confirms the lower recombination rate for the PDPB/SnO_2 composites. When solar light is irradiated on the PDPB/SnO_2 heterojunction, the photogenerated electrons can be easily excited from the PDPB valence band (VB) to the conduction band (CB) and subsequently injected to the CB of SnO_2 MSCs. Moreover, the hole still remains in the valence band of PDPB. Then, the electrons and holes further react with O_2 or H_2O to generate the superoxide radical and hydroxyl radicals, and these radicals can oxidize the RhB and degrade it,
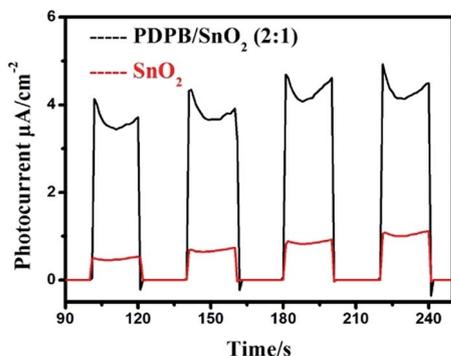

Fig. 8 Photocurrent spectra of pure SnO_2 MSCs (red) and PDPB/SnO_2 composites (black) (2 : 1).
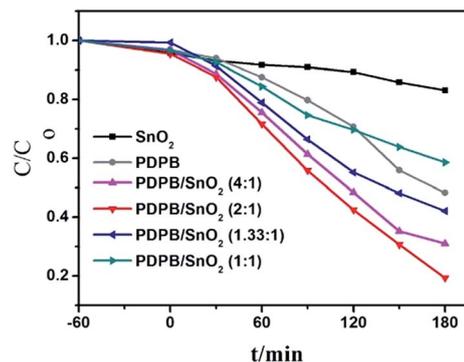

Fig. 9 Photodegradation of RhB of pure PDPB, pure SnO_2 and PDPB/SnO_2 composites under the solar light irradiation (Xe lamp with AM1.5 filter).

which is in accordance with the highly photocatalytic activity of PDPB/SnO_2.

3.7 Photocatalytic activity measurement

The photocatalytic activity of the as-prepared samples was evaluated by measuring the decomposition rate of the model pollutants of Rhodamine B (RhB) in water under solar light (Xe lamp with AM1.5 filter). The photocatalytic activities at different ratios of PDPB/SnO_2 were compared with the activities of pure PDPB and pure SnO_2 MSCs. Fig. 9 shows the degradation rate of all samples, and it is clearly shown that all PDPB/SnO_2 composites presented an evidently enhanced photocatalytic activity than pure SnO_2 MSCs. The samples with 4 : 1, 2 : 1, and 1.33 : 1 ratios also showed a photocatalytic activity higher than the pure PDPB. The SnO_2 MSCs with a wide band gap showed a low solar light activity to degrade RhB. The p–n heterojunction showed a much higher photocatalytic activity that is caused due to the sensitization of PDPB and the narrowed band gap of SnO_2 resulting due to carbon doping. The PDPB/SnO_2 showed a higher activity than pure PDPB owing to the synergistic effect of the p–n heterojunction and PDPB sensitization. That is, the photo-generated electrons and holes have an efficient separation at the interface between PDPB and the SnO_2 MSCs. The 2 : 1 ratio sample had the highest photocatalytic activity, whose degradation rate of RhB is 4 times and 2 times that of pure SnO_2 MSCs and pure PDPB, respectively. The sample with a 1 : 1 ratio showed a relatively lower activity, which indicates that the extra PDPB covered on the surface of SnO_2 would decrease the light absorption of C–SnO_2. Therefore, the ratio of PDPB and SnO_2 MSCs has an optimum value. In addition, the PDPB amount in the PDPB/SnO_2 (1 : 1) composite is relatively low (lower than 8%), and hence the main body of the PDPB/SnO_2 composite is SnO_2. Thus, the composite with 1 : 1 ratio shows a lower activity than PDPB. When the amount of PDPB is too high, it generates more recombination centers of electrons and holes. This indicates that the ratio of PDPB and SnO_2 has an optimal value.

3.8 Mechanism

The proposed mechanism of the PDPB/SnO_2 heterojunction is illustrated in Fig. 10. In this heterojunction structure, n-type SnO_2 MSCs provided a stable mesoporous structure,
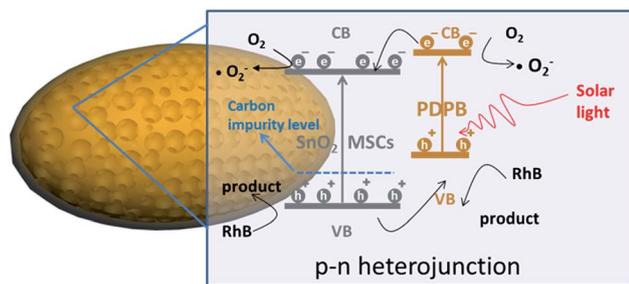
Fig. 10 Mechanism of the PDPB/SnO$_2$ composite degradation of the RhB under solar light.

a hydrophilic environment, a high electron mobility, and exposed facets with active sites, which could expedite the electron transfer rate. The p-type PDPB on the surface of the heterojunction acted as a sensitizer to improve the solar light absorption.[31] The generation of Sn–C bonds between SnO$_2$ and PDPB introduced a carbon impurity level above the VB of SnO$_2$, which led to the solar light response of SnO$_2$. The construction of a p–n heterojunction provided an ohmic interface to enhance the separation of photogenerated electrons and holes.

4. Conclusion

In summary, we used an *in situ* strategy to synthesize a PDPB/SnO$_2$ p–n heterojunction that exhibited a high photocatalytic activity for the degradation of RhB under solar light irradiation owing to its excellent light harvesting and effective separation of electrons and holes. The chemical bonds of Sn–C generated on the interface of heterojunctions could decrease the bandgap of SnO$_2$ and enhance the interaction between the two components. As a result, the as-prepared catalysts had a high solar-driven photocatalytic performance. Our study gives a facile strategy for the preparation of an organic–inorganic hybrid heterojunction with high solar light activity.

Acknowledgements

Notes and references

1 Z. Zhu, X. Zheng and Y. Bai, *Phys. Chem. Chem. Phys.*, 2015, **17**(28), 18265–18268.
2 X. Zheng, Q. Kuang, K. Yan, Y. Qiu, J. Qiu and S. Yang, *ACS Appl. Mater. Interfaces*, 2013, **5**, 11249–11257.
3 E. J. W. Crossland, N. Noel, V. Sivaram, T. Leijtens, J. A. Alexander-Webber and H. J. Snaith, *Nature*, 2013, **495**, 215–219.
4 W. Jiao, Y. Xie, R. Chen, C. Zhen, G. Liu, X. Ma and H.-M. Cheng, *Chem. Commun.*, 2013, **49**, 11770–11772.
5 S. Bao, Z. Wang, X. Gong, C. Zeng, Q. Wu, B. Tian and J. Zhang, *J. Mater. Chem. A*, 2016, **4**, 18570–18577.
6 Z. Yu, X. Wu, J. Wang, W. N. Jia, G. S. Zhu and F. Y. Qu, *Dalton Trans.*, 2013, **42**, 4633.
7 A. Biaggi-Labiosa, F. Sola, M. Lebŕon-Coĺon, L. J. Evans, J. C. Xu and G. W. Hunter, *Nanotechnology*, 2012, **23**, 455501.
8 F. Song, H. L. Su, J. Han, W. M. Lau, W. J. Moon and D. Zhang, *J. Phys. Chem. C*, 2012, **116**, 10274–10281.
9 Y. Jia, L. F. He, Z. Guo, X. Chen, F. L. Meng, T. Luo, M. Q. Li and J. H. Liu, *J. Phys. Chem. C*, 2009, **113**, 958.
10 L. Etgar, P. Gao, Z. S. Xue, Q. Peng, A. K. Chandiran, B. Liu, M. K. Nazeeruddin and M. Gratzel, *J. Am. Chem. Soc.*, 2012, **134**, 17396.
11 S. Gubbala, V. Chakrapani, V. Kumar, *et al.*, *Adv. Funct. Mater.*, 2008, **18**(16), 2411–2418.
12 C. B. Fitzgerald, M. Venkatesan and A. P. Douvalis, *J. Appl. Phys.*, 2004, **95**(11), 7390–7392.
13 Y. Zhao, Y. Zhang, J. Li and Y. Chen, *Sep. Purif. Technol.*, 2014, **129**, 90–95.
14 W. A. Badawy and H. H. Afify, *J. Electrochem. Soc.*, 1990, **137**(5), 1592–1595.
15 D. Liu and P. V. Kamat, *J. Electrochem. Soc.*, 1995, **142**(3), 835–839.
16 G. D. Wang, C. P. Wei and R. Y. He, *Mater. Sci. Forum*, 2016, **852**, 1112–1117.
17 N. D. M. Sin, M. F. Malek and M. H. Mamat, *Int. J. Mater. Eng. Innovat.*, 2014, **5**(2), 159–170.
18 Y. C. Zhang, L. Yao, G. Zhang and D. D. Dionysiou, *Appl. Catal., B*, 2014, **144**, 730–738.
19 M. T. Mayer, Y. Lin, G. Yuan and D. W. Wang, *Acc. Chem. Res.*, 2013, **46**, 1558–1566.
20 J. S. Jang, H. G. Kim and J. S. Lee, *Catal. Today*, 2012, **185**, 270–277.
21 A. Kongkanand, K. Tvrdy, K. Takechi, M. Kuno and P. V. Kamat, *J. Am. Chem. Soc.*, 2008, **130**, 4007–4015.
22 D. R. Baker and P. V. Kamat, *Adv. Funct. Mater.*, 2009, **19**, 805–811.
23 Y. Wang, *Nanoscale*, 2013, **5**, 8326–8339.
24 L. Zhang, H. Zhang and H. Huang, *New J. Chem.*, 2012, **36**(8), 1541–1544.
25 L. Zheng, Y. Zheng and C. Chen, *Inorg. Chem.*, 2009, **48**(5), 1819–1825.
26 Z. Zhang, C. Shao and X. Li, *J. Phys. Chem. C*, 2010, **114**(17), 7920–7925.
27 S. Ghosh, N. A. Kouamé and L. Ramos, *Nat. Mater.*, 2015, **14**(5), 505–511.
28 X. Zheng, Y. Lv and Q. Kuang, *Chem. Mater.*, 2014, **26**(19), 5700–5709.
29 G. Neri, C. Milone and S. Galvagno, *Appl. Catal., A*, 2002, **227**(1), 105–115.
30 S. Sardar, P. Kar and H. Remita, *Sci. Rep.*, 2015, **5**, 17313.
31 J. Lei, L. Yang, D. Lu, X. Yan, C. Cheng, Y. Liu, L. Wang and J. Zhang, *Adv. Opt. Mater.*, 2015, **3**, 57–63.